Solar Energy 274 (2024) 112602

Contents lists available at ScienceDirect

Solar Energy

journal homepage: www.elsevier.com/locate/solener

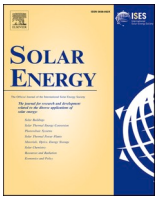

Perovskite photovoltaics for aerospace applications – life cycle assessment and cost analysis

Guangling Zhao *, Declan Hughes, David Beynon, Zhengfei Wei, Trystan Watson, Wing Tsoi Chung, Jenny Baker

Faculty of Science and Engineering, Swansea University, Swansea, Wales, the UK

ARTICLE INFO

Keywords:
Perovskite photovoltaics
Aerospace applications
Life cycle assessment
Cost analysis

ABSTRACT

In the past few years, we have witnessed a rapid evolution of perovskite solar cells. In this study, we employ life cycle assessment (LCA) to identify the potential environmental impacts of perovskite solar cells (PSC) optimised for aerospace applications but could be used in conventional terrestrial applications too. One PSC module is manufactured by spin coating equipped with ITO glass and gold cathode. The other PSC module is manufactured by slot-die coating with a PET layer and carbon cathode and gold cathode respectively. Life cycle assessment is employed to compare potential environmental impact of two manufacture methods by impact method of Recipe (H), as well as the fabrication cost of PSC module. The primary data of material and energy used for fabricating PSCs are collected from spin coating with lab scale and slot-die coating with pilot scale. The life cycle impact assessment of the PSC module in the pilot scale shows much lower in all the assessed 18 impact categories than in the lab scale thanks to the material use efficiency and reducing energy consumption. Gold as a conduct electrode has the highest impacts in both spin coating and slot-die coating modules. Calculating with a two-year lifetime (typical of aerospace applications), the impact of global warming potential from the PSC module with carbon electrode with pilot scale used in a terrestrial application is calculated to be 12 g/kWh.

1. Introduction

The past 10 years have witnessed a rapid evolution of perovskite solar cells (PSC), going from a short-lived device with liquid electrolyte into a promising solar technology. Since the first published work in 2009 [31], the PSC devices have been increasing their lifetimes to 10,000 h [22]and efficiencies of over 25 % for single junction devices [58], and almost 32.5 % for tandem devices [28]. The high specific power of perovskites has led to these devices being considered for space applications [51]. While the efficiencies of PSCs are increasing, more researchers have investigated scaling up PSCs [9,18,34], along with assessing targeted and promising applications for the use of PSCs. One of the applications highlighted where perovskite solar cells have potential is their use in aerospace applications to replace gallium arsenide-based tandems which have high cost, high materials impact and lower power density than perovskites [26]. Reese et al 2018 have estimated the total aerospace market to be 5 MW per annum, growing to a range of 260–500 MW per annum in 2028 [42,56].

Aerospace applications are divided into atmospheric (drones etc.), stratospheric (>20 km for the earth's surface) e.g., high altitude pseudo satellites (HAPS) and space typically defined as > 100 km. Whilst they have different environmental demands, they have a common need to prioritize power density at the expense of cost. HAPS applications operate at about 20–30 km in a near earth orbit [20]. The environment in which the HAPS operates has a wide temperature range of over 150 °C and solar radiation of AM0 (e.g. ultraviolet rich) 1366.1 W/m^2, compared with a standard of AM1.5 1000 W/m^2 on earth [26].

A typical annual irradiance experienced by a device at a height of 20 km can be three times the equivalent location on Earth [46]. The leading space applications use a rigid, thick, and heavy structure (AZUR [3], along with rigid solar cells such as the AlInGaP/AlInGaAs/InGaAs/Ge devices from Azur Space [47]. While the performance of these multi-junction SCs is power conversion efficiency (PCE) (31.8 %), due to the thickness of the solar cells (100 μm), they offer a low specific power ~0.4 Wg^{-1}. Additionally, the fabrication processes used to manufacture these devices are expensive and utilise materials with high scarcity [25]. These factors showcase why new materials and PV technologies are needed to replace the current technology. Furthermore, PSCs are of particular interest for space applications because the perovskite active layer exhibits a high radiation resistance compared with III-V SCs

* Corresponding author.

https://doi.org/10.1016/j.solener.2024.112602
Received 25 September 2023; Received in revised form 30 January 2024; Accepted 6 May 2024
Available online 9 May 2024

[5,27,51]. PSC devices being tested for aerospace capability are currently being manufactured at lab scale using spin coating however this fabrication technique limits the practical scale-up size of these devices to 100 cm^2 [26]. Roll-to-roll (R2R) fabrication of PSCs has the potential for large area, low weight, and flexibility [48]. These properties are fundamental for the realization of roll-out solar arrays. Thus, assessing the cost of fabricating large-area PSCs in relation to their performance is fundamental to establishing their potential as a disruptive technology in the space sector.

There have been several cost analyses and comments performed on perovskite solar cells [16,17,41,45]. Given the pre-production stage of the technology, these can only be estimates and are all calculated using a bottom-up approach. Whilst different works focus on different architectures and transport layers, they all have a commonality that the electrodes (both the transparent one and the opaque contact) are significant proportions of the cost and therefore increasing the efficiency of devices results in a drop in price per kWp.

It is important to understand the potential environmental impacts of PSC devices as well as the cost. LCA studies of PSC devices have covered different materials and architectures [11]. The focus for terrestrial application has been primarily on global warming potential (GWP) due to the use of solar to support CO_2 emissions reductions, and the Green Electronics Council (GEC) defines the requirements for an ultra-low carbon emissions solar cell as 400 kg CO_2-eq/kWp [23]. The potential impact from increased material use as we move to net zero has been highlighted as an issue [60], and for this reason metal depletion potential (MDP) is one of the impacts highlighted in extra detail within the study, alongside human toxicity potential (HTP), terrestrial ecotoxicity potential (TEP) and GWP. Whilst the utilisation of photovoltaics in satellite applications is unlikely to reach the volumes used in terrestrial applications their use is growing (Hughes 2022) and therefore it is important to minimise environmental impacts.

The objective of this study is to assess the potential environmental and economic assessment of PSC developed for aerospace application. The spin coated devices assessed in this article have been optimised and tested in our laboratories for aerospace applications (Hughes 2022) and the slot-die device is a modified spin coated architecture ensuring suitability for aerospace applications where the focus is on energy and power density as well as radiation hardness.

The structure of this article is organised as below. In section 2, the material and architecture of PSC are explained followed by manufacture techniques. In section 3 the assessment methods of LCA and cost analysis are explained. In section 3, the results of both environmental and economic assessment of PSC are presented. The sensitivity analysis of alternative materials is conducted from environmental and cost perspectives in section 4.

2. Perovskite architecture and fabrication

2.1. PSC module

The structure of PSC consists of sputtering-coated ITO (indium doped tin oxide) coated glass substrate (Fig. 1(a)), ITO-coated polyethylene terephthalate (PET) (Fig. 1(b, c), a Tin Oxide electron transport layer, a triple cation perovskite absorber, a Spiro-OMeTAD hole transport layer, and a gold contact layer (Fig. 1(a,b)). The slot-die coating architecture has equivalent layers except for the substrate where polyethylene terephthalate (PET) replaces glass, and a carbon layer replaces gold as the contact layer (Fig. 1(c)).

2.2. Fabrication process

The manufacturing process is described step by step both in the lab by spin coating (Fig. 2) and in pilot-scale production by R2R slot die (Fig. 3). For the spin coated device the method (Glass/ITO/SnO2/Triple Cation/Spiro/Au) and subsequent cell performance is described by Barbé [4]. ITO + glass substrates (supplied by Kintec, Hong Kong) were cleaned by ultra-sonication in Hellmanex (2 %, deionized water) for 5 min, then further sonicated with deionized water for 15 min, acetone for 10 min, and then 2-propanol for 5 min before being dried via a N_2 and then treated in oxygen plasma for 5 min. A planar layer of SnO_2 (~25 nm) was deposited via spin-coating at a spin speed of 3000 rpm and an acceleration of 3000 rpm for 30 s. The SnO_2 precursor solution was fabricated from commercial tin oxide nanoparticles (15 % colloidal dispersion in H_2O; Alfa Aesar) diluted in deionized water (1:6.5, v:v). This was sintered the substrates at 150C for 30 min in a fume hood. Triple-cation perovskite films were deposited in an N_2 atmosphere using single-step deposition method from the precursor solution containing FAI (172 mg) (Dyesol), PbI_2 (507 mg) (TCI), MABr (22 mg) (Dyesol), and $PbBr_2$ (73 mg) (TCI) in anhydrous N,N-dimethyl formamide (99.8 %; Sigma-Aldrich)/ dimethyl sulphoxide (99.7 %; Sigma-Aldrich) (8:2 v:v). Thereafter, 53 μL of CsI (99.999 % trace metal; Sigma-Aldrich) (390 mg, 1 mL DMSO) was added to the precursor solution. The precursor solution was spin-coated onto the planar SnO_2 films [26]. To complete the fabrication of devices, 2,20,7,70-tetrakis(N,N-di-p-methoxyphenylamine)- 9,9-spirobifluorene (Spiro-OMeTAD; 90 mg in chlorobenzene) as a hole transporting material was deposited by spin-coating 100 μL of the prepared solution at 4000 rpm for 20 s. Spiro-OMeTAD (Sigma-Aldrich) was doped with bis(trifluoromethane)sulfonimide lithium salt (99.95 %; Sigma-Aldrich) dissolved in acetonitrile (520 mg/ml), tris(2-(1H-pyrazol-1-yl)-4-tertbutylpyridine)-cobalt(III)-tris(bis(trifluoromethylsulfonyl)imide) dissolved in acetonitrile (300 mg/ml FK 209; from Dyenamo) and 4-*tert*-butylpyridine (96 %; Sigma-Aldrich) with concentrations of 34, 10, and 19 μL, respectively. Finally, device

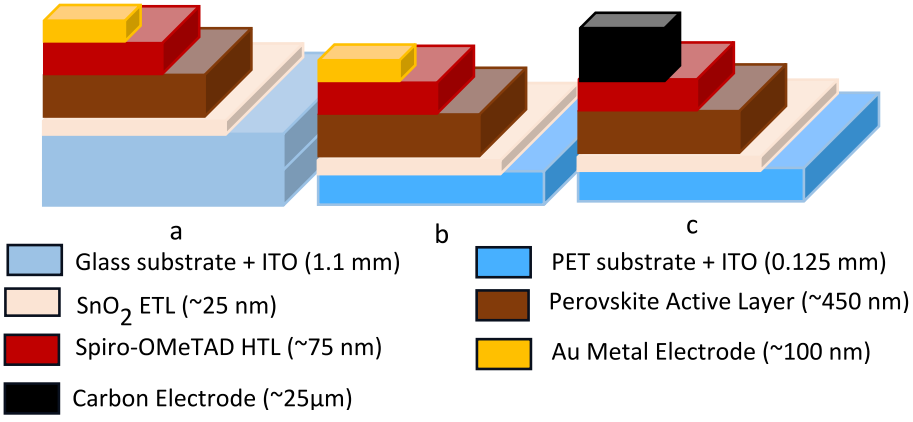

Fig. 1. Structure of PSC module analysed in Section 3 (a) Spin coating with gold contact architecture (b) Slot-die coating with gold contact architecture, (c) Slot-die coating with carbon contact architecture.

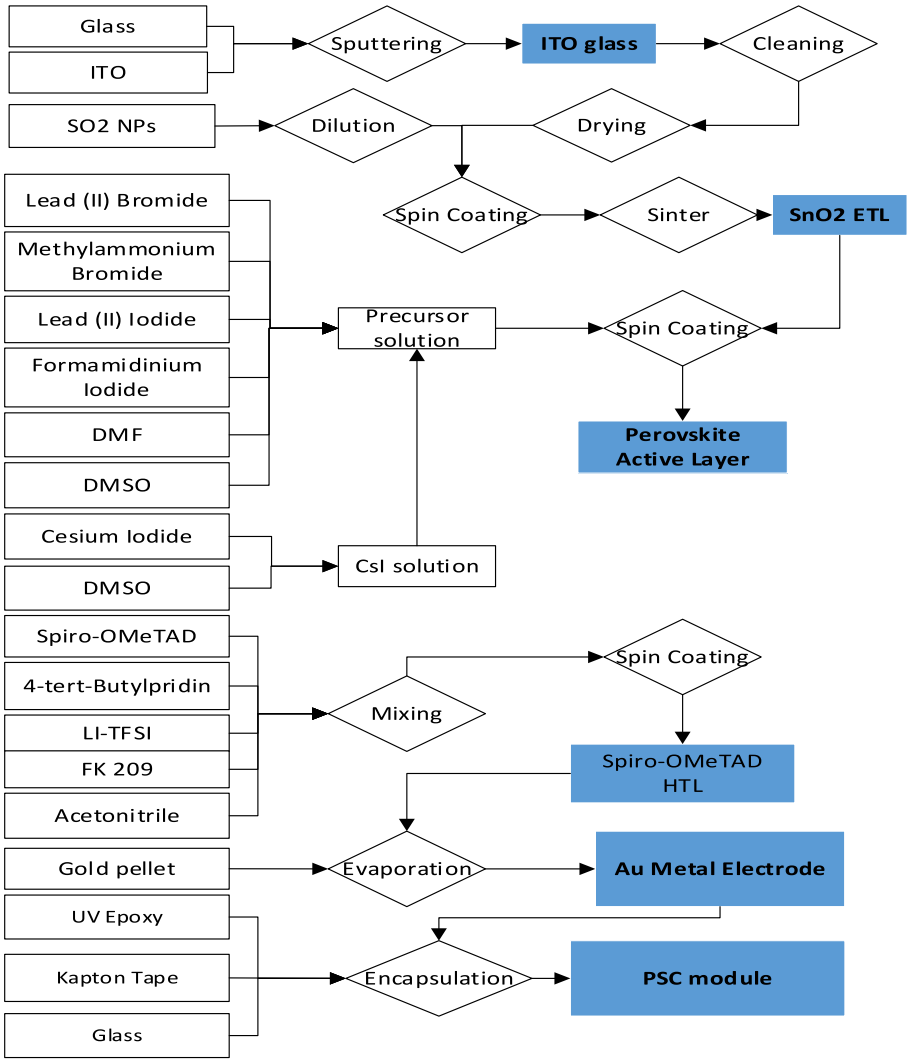

Fig. 2. Flow diagram of the fabrication process of the PSC module in the lab.

fabrication was completed by thermally evaporating gold wire (99.9 % 1 mm; Kurt J.Lesker) to form a ~100 nm gold layer as a back contact.

Pilot scale device produced by slot-die coating has not been conducted for this specific device architecture due to the toxicity of the solvent system used for the perovskite and the cost of the spiro-OmeTAD ink. To make a comparison a slot-die coating fabrication process is envisaged based on previous experience of roll-to-roll (R2R) coating alternative perovskite and hole transport materials and the formulation and coating parameters of roll to roll coated SnO_2 and carbon electrode [11,50]. Further details of the fabrication process and subsequent performance are described by Beynon [6]. It is therefore assumed that tin oxide (15 % colloidal solution Alpha Aesar) was diluted to 1.2 % with DI water and 10 % 1-Butanol then coated onto 50 Ω/sq ITO coated PET using a Cotema Smartcoater R2R coating system. The tin oxide is coated at 7 μm wet film thickness using a 1 mm meniscus guide and 200 μm gap at 90 mm coating width and 140 °C drying temperature. Next, the perovskite layer is coated using the same formulation as spin-coated devices with 5 μm wet film thickness, 90 mm coating width, and 1 mm meniscus guide with a 200 μm gap. Immediately following coating an air knife is used to dry the perovskite with 50 l/min flow rate of dry nitrogen then annealed at 150 °C. Next, the Spiro-OMeTAD is coated using the same formulation as for spin-coated devices using 4 μm wet film thickness and 90 mm coating width 500 μm meniscus guide and 150 μm gap.

This study considers two types of top electrodes for the slot-die coated device. Firstly, a gold top contact is evaporated in the same method as the lab-based device after the R2R module has been cut to size (Fig. 3) [8]. Secondly carbon ink is formylated with ethylcellulose, 2-methylanisole, carbon black, and graphite [6]. A carbon top contact is considered which is coated in 12 stripes each 4 mm wide with 250 μm wet film thickness and oven temperature of 140 °C. All layers are coated at a speed of 1 m/min and oven residence time of 1 min. In the scenario where an industrial process is used but then a gold top contact is evaporated onto the module rather than the carbon top contact.

3. Method

3.1. Goal and scope definition

Following ISO 14044, the first step is to define the goal of this study. The goal of this study is to assess the potential environmental and economic profile of different substrates and techniques of manufacturing perovskite for aerospace applications. To achieve the goal, a holistic methodology of life cycle assessment (LCA) and life cycle cost (LCC) is employed. The cost covers the cost of the equipment, the energy cost for manufacture, and the material cost including logistics. In this study, environmental and economic impact analysis are based on the perovskite solar cell designed for aerospace applications however the architecture is such that it could also be used in standard terrestrial applications. The functional unit (FU) of this study is 1 m^2 of the PSC

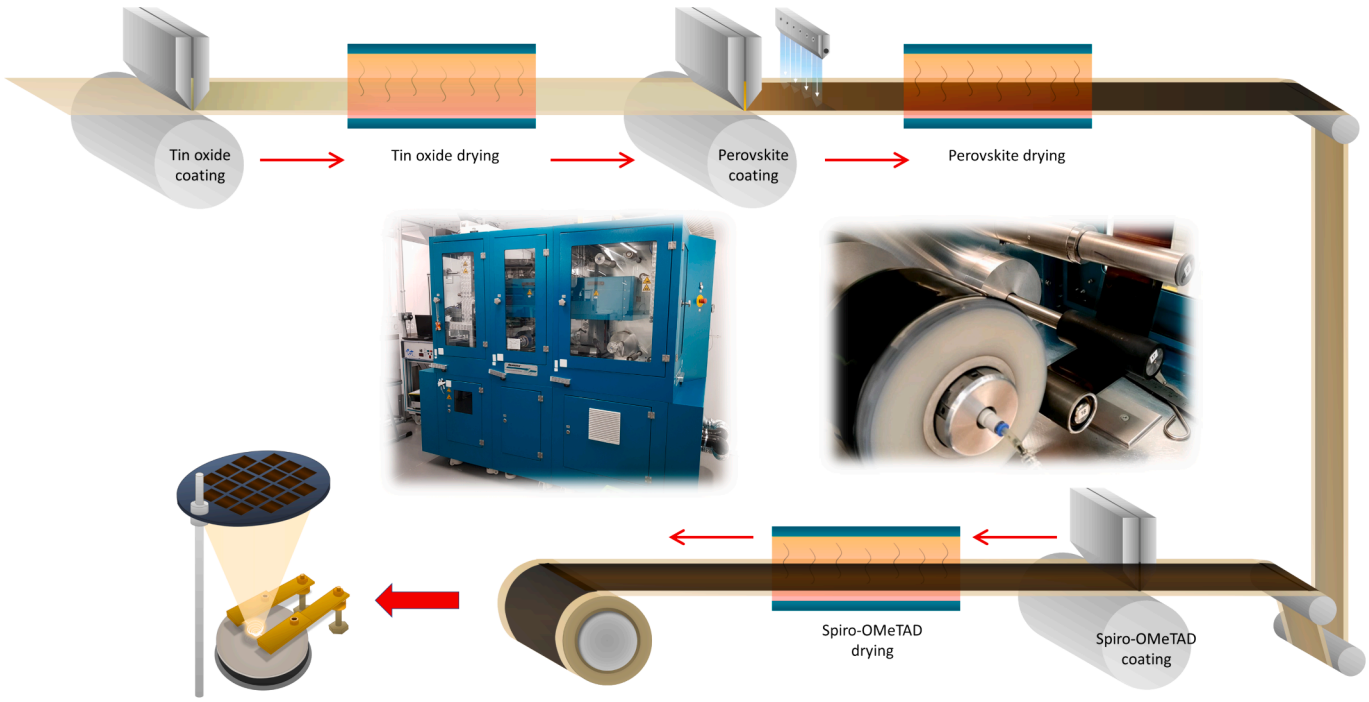

Fig. 3. Schematic visualisation of R2R slot-die coating method for fabrication of PSCs with gold top electrode.

module. To allow comparison with other PV technologies an Excel sheet is supplied in Supplementary Material A which enables adjustment of cell lifetime, irradiance, efficiency, and geometrical fill factor to allow the functional unit to be converted to kWp or kWh over the device lifetime.

The system boundary includes the material acquisition, and material transportation, and fabrication process in the UK, and the PSC operation in space. In the lab spin coating fabrication, the material bought from EU counties, is transported by lorry and road transport. In the pilot slot-die fabrication, the material bought from China, is transported firstly by sea then land transports. The PSC fabrication process is operated in the UK using UK electricity. The UK electricity mix is based on the report from National Energy System Operator (NESO)NESO. National Energy System Operator. [38]. The cost analysis includes the machine cost and material cost including shipping. Labor cost and maintenance cost, and land cost etc. are not included in current analysis.

3.2. Life cycle and economic inventory

After defining the goals and scope of the study, a life cycle inventory (LCI) is compiled, which includes all materials used and energy consumed within the product life cycle system boundary. We collected data directly from PSC scientists and manufacturers, which includes material used and energy inputs for fabrication. Each layer of the device is made from the material presented in Table 1. In the laboratory fabrication, the structure of perovskite includes ITO glass, SnO_2 nanoparticles, triple cation perovskite, spiro-OMeTAD, gold metal contacts and glass encapsulation layers. The material input is the amount which is used for the fabrication. The material utilisation efficiency is calculated from material used in the solar cell versus the material input. In slot-die coating fabrication, the structure of perovskite includes ITO + PET, SnO_2 nanoparticles, triple cation perovskite, spiro-OMeTAD, carbon contacts and glass encapsulation layers. One advantage of the R2R slot-die is the material utilisation efficiency of over 99 % with yield loss only at the beginning and end of a coating run.

The economic inventory includes machine costs for producing solar cells (equipment) and manufacture cost (material and energy only) (Table 2). The cost of material and equipment is the market selling price, which includes a shipping fee. The cost considered in this study is depreciation cost and normalised per m^2 of production output, which is calculated by dividing the capital cost of equipment by its lifetime in hours and then multiplying by the running time to produce 1 m^2. The cost of labour, maintenance, and R&D is not included in current cost analysis. All operations are performed using electric equipment, so electricity is the only energy consumption, which is collected by the direct measuring of electricity usage through machine.

The material use and energy consumption are collected directly from the fabrication process. In this study, the spin coating fabrication is carried out in small scale, which determined the volume of material need is small amount. For material cost with small volume, the cost is obtained from two supplier of Merck(https://www.sigmaaldrich.com) and Ossila (https://www.ossila.com/). The material cost with industrial volume, the cost is obtained from Made-in-China (https://www.made-in-china.com/) and Alibaba(https://www.alibaba.com/). The equipment investment is purchasing price including shipping and installation fee.

3.3. Life cycle impact assessment

After the LCI is created, the contribution of each of the individual entries toward various impact categories is calculated during the impact assessment (LCIA). In this study, the LCIA method is Recipe 2016 (H). All 18 mid-point impact categories are analysed and compared (Table 3). The software used to carry out the calculations is Gabi with the database of Ecoinvent V3.8.

4. Environmental and economic assessment results

4.1. Environmental profile

Table 4 presents the LCIA of the PSC module from the current laboratory deposition method in comparison to the proposed pilot manufature method. The first comparison is in a functional unit of m^2, for the lab scale with gold electrode, R2R slot-die with gold electrode, and R2R slot-die with carbon electrode. The efficiencies of the studied modules are 22 %, 18 %, and 15 % respectively. The active area is 80 % of the

Table 1
Material inventory and cost of 1 m^2 of encapsulated PSC module.

layers	Spin coater-lab scale		Slot-die coating-pilot scale	
	material (g)	cost (€)	material (g)	cost (€)
Substrate + TCO				
ITO − Glass	2,770.0	4,300.0		
PET −Polyethylene terephthalate			172.5	0.2
ITO			0.7	0.6
Di water	7,676.0	2.1		
Hellmanex 2 % in DI water	1,400.0	146		
SO_2 NPs layer				
SO2 NPs	0.2	0.02	1.8	3.9E-03
Di Water	1,780.0	0.5	2.9	8.1E-04
1-Butanol			0.2	2.8E-04
Triple Cation Perovskite				
Lead (II) Iodide	308.0	838.0	3.1	0.04
Lead (II) Bromide	44.4	261.0	0.4	0.01
Methylammonium Bromide	13.4	290.0	0.1	1.5E-03
Formamidinium Iodide	105.0	1,660.0	1.1	0.48
DMF-Dimethylformanide	459.0	256.0	4.6	4.3E-03
DMSO-Dimethyl sulfoxide	162.0	159.0	1.7	0.01
Cesium Iodide	9.9	91.8	0.1	2.2E-03
chlorobenzene (CB) (C6H5Cl)	480.0	44.5	30.0	0.1
Spiro-OMeTAD				
Spiro-OMeTAD	14.4	4,516.0	0.051	16.1
Chlorobenzene	160.0	14.8	0.6	2.2E-03
4-*tert*-Butylpyridin	5.4	19.5	1.8E-02	0.06
LI-TFSI	1.6	6.4	5.6E-03	6.5E-05
Acetonitrile	3.0	0.1	0.013	2.2E-05
FK209	4.8	211.8	1.8	0.8
Acetonitrile	1.6	0.05	0.1	1.2E-03
Gold/Carbon Contact layer				
Gold pallet	8.9	357.6	2.1	106.2
Graphite			27.5	0.03
2-Methylanisole			295.3	0.01
Carbon black			10.6	0.01
Ethylcellulose			17.2	0.5
Glass Encapsulation				
Glass	2080.0	1.7		
polyimide tape	16.0	0.01		
UV-Cured Epoxy	32.0	0.1		
Poly(methyl methacrylate) (PMMA)			14.0	0.03

whole module. The insolation per year is set to be 1000 kWh/m^2. The lifetime is assumed to be 2 years, limited by the useful life of the satellite. Supplementary A is a spreadsheet including this calculation where the reader can adjust the insolation, efficiency, lifetime and active area to compare against the reference flows of other devices reported in literature.

In the R2R slot-die fabrication process, it can be seen that the impacts are typically 1 order of magnitude lower than the lab-based method if the top contact is gold and 3 orders of magnitude lower than if the top contact is carbon materials. This is for several reasons, firstly slot-die deposition is significantly less wasteful than the spin coating deposition. Secondly, the glass substrate and gold contact is replaced by PET substrate and carbon contact in order to enable the devices to be manufactured using a scaleable process. Finally, the lab-based process is not optimised, f.x. it can be seen that the ultrasonic bath cleaning requires almost 66 kWh of electricity per m^2 of substrate cleaned due to the long length of time the samples are in the bath which is quite small so does not hold much material at once. This could likely be reduced significantly if an optimisation study was performed and it is advised researchers perform such studies to reduce the environmental impacts of

Table 2
Energy consumption and cost for manufacturing 1 m^2 PSC encapsulated module.

Energy consumption and cost	Energy consumption (kWh)	cost (€)	Capital investment (Thousand €)	Depreciation cost / m^2 (€)
ITO Glass layer				
Ultrasonic Bath	66.0	22.2	1.4	34.6
nitrogen dry gun	16.0	5.4		
Coatema Smartcoater	1.2	0.4	168.0	0.06
SO_2 NPs layer				
Spin coater	0.6	0.2	3.1	0.3
Hot plate	1.8	0.6	0.5	0.7
Coatema Smartcoater *inc drying*	1.2	0.4	168.0	0.06
Triple Cation Perovskite				
UV ozone cleaner	16.0	5.4	3.4	6.0
Spin coater	6.4	2.2	3.1	240.8
Hot plate	1.5	0.5	0.5	57.8
Coatema Smartcoater *inc drying*	1.2	0.4	16.0	0.06
Spiro-OMeTAD				
Spin coater	0.4	0.1	3.1	0.2
Coatema Smartcoater *inc drying*	1.2	0.4	168.0	0.06
Gold/Carbon Contact layer				
low-temperature evaporation of gold	0.03	9.0E-03	44.8	0.04
carbon contact layer Coatema Smartcoater *inc drying*	1.2	0.4	168.0	0.06
Glass Encapsulation				
Coatema Smartcoater	1.2	0.4	168.0	0.06
Solar Cell Laser Scribing Machine	0.5	0.2	112.0	0.03

Table 3
Mid-point impact categories.

Mid-point impact category	Abbreviation	unit
Climate change, incl. biogenic carbon	GWP	kg CO_2-eq.
Fine Particulate Matter Formation	FPMF	kg $PM_{2.5}$-eq.
Fossil depletion	FDP	kg oil-eq.
Freshwater Consumption	FCP	m^3
Freshwater ecotoxicity	FETP	kg 1,4-DB −eq.
Freshwater Eutrophication	FEP	kg P-eq.
Human toxicity, cancer	HTP cancer	kg 1,4-DB-eq.
Human toxicity, non-cancer	HTP non-cancer	kg 1,4-DB-eq.
Ionizing Radiation	IRP	Bq, C-60-eq. to air
Land use	LUP	Annual crop-eq. yr
Marine ecotoxicity	METP	kg 1,4-DB-eq.
Marine Eutrophication	MEP	kg N-eq.
Metal depletion	MDP	kg Cu-eq.
Photochemical Ozone Formation, Ecosystems	POFP-eco	kg NO_x-eq.
Photochemical Ozone Formation, Human Health	POFHP-hum	kg NO_x-eq.
Stratospheric Ozone Depletion	SODP	kg CFC-11-eq.
Terrestrial Acidification	TAP	kg SO_2-eq.
Terrestrial ecotoxicity	TETP	kg 1,4-DB-eq.

Table 4
LCIA results of PSC module per m^2 for PSC module based on lab scale, pilot scale with gold electrode and pilot scale with carbon electrode.

Impact category	Unit	Spin coater-lab scale			Sot-die with gold electrode-pilot scale			slot-die with carbon electrode-pilot scale		
		per m^2	per kWp	Per kWh	per m^2	per kWp	Per kWh	per m^2	per kWp	Per kWh
GWP	kg CO2-eq.	570.3	3240.5	1.6	105.0	15.1	0.4	3.0	0.4	0.01
FPMF	kg PM2.5-eq.	1.3	0.2	0.4	0.3	0.04	1.0E-3	5.0E-3	1.0E-3	2.3E-5
FDP	kg oil-eq.	227.5	40.0	0.6	38.8	5.6	0.1	1.7	0.2	7.3E-3
FCP	m3	5.1	0.9	0.01	1.0	0.1	4.0E-3	0.02	2.4E-3	8.2E-5
FETP	kg 1,4-DB −eq.	622.9	109.6	1.8	147.3	21.2	0.5	0.4	0.05	2.0E-3
FEP	kg P-eq.	1.6	0.3	5.0E-3	0.4	0.05	1.0E-3	1.3E-3	5.6E-4	6.8E-5
HTP cancer	kg 1,4-DB-eq.	60.5	10.6	0.2	12.4	1.8	0.04	0.1	0.02	1.0E-3
HTP non-cancer	kg 1,4-DB-eq.	4792.2	843.4	13.6	3305.8	476.0	11.5	3.6	0.4	0.02
IRP	Bq, C-60-eq. to air	74.4	13.1	0.2	11.8	1.7	0.04	1.1	0.1	4.0E-4
LUP	Annual crop-eq.yr	37.1	6.5	0.1	7.1	1.0	0.02	0.2	0.02	1.0E-5
METP	kg 1,4-DB −eq.	793.1	139.6	2.3	187.1	26.9	0.6	0.1	0.01	1.0E-3
MEP	kg N-eq.	0.03	5.6E-3	9.1E-5	6.9E-3	9.9E-4	2.4E-5	1.1E-4	1.4E-5	4.9E-7
MDP	kg Cu-eq.	57.3	10.1	0.2	11.6	1.7	0.04	0.6	0.1	3.0E-3
POFP-eco	kg Nox-eq.	2.7	0.5	7.8E-3	0.6	0.08	2.0E-3	0.01	1.8E-3	6.1E-5
POFHP-hum	kg Nox-eq.	2.7	0.5	7.7E-3	0.6	0.1	2.0E-3	0.01	1.6E-3	5.7E-5
SODP	kg CFC-11-eq.	3.7E-4	6.6E-5	1.1E-6	7.3E-5	1.0E-5	2.5E-7	2.2E-6	2.6E-7	9.2E-9
TAP	kg SO2-eq.	3.0	0.5	8.5E-03	0.6	9.0E-2	2.2E-3	0.01	1.9E-3	6.5E-5
TETP	kg 1,4-DB-eq.	1785.7	3.14.3	5.1	490.3	7.06	1.7	9.9	1.2	0.04

their research. For this reason, the pilot scale-based method is much more representative of the anticipated impacts of these devices should they be manufactured commercially.

Spin coated devices have a GWP impact of 94 kg CO_2 −eq/kW_p, when the pilot scale slot-die coating process is used but still with a gold top contact, this is reduced to 15 kg CO_2-eq/kW_p which then further reduces 0.4 kg CO_2-eq/kW_p, when a carbon top contact replaces the gold in the slot-die coating device. This is significantly lower than the impact reported by Alberola-Borras [1]who was also analysing devices made in the same lab and reported an impact of 165 g CO_2-eq/kWh which was calculated as 18 kg CO_2-eq/kW_p. The reason for this cannot be explained solely by the reduction of the UK grid carbon intensity from 2017 to 2022 which was reduced by 15 % during this period. The explanation is that a very different screen-printed PSC architecture was assessed by Alberola-Borràs which had multiple 450 °C sintering processes[37]. The perovskite was was dispersed through a 10 μm carbon layer, drying time was 50 min rather than 2 min which contributed significantly to the electricity impacts. In addition, the substrate was 2.2 mm thick glass rather than 125 μm PET. This demonstrates that the lightweight undertaken to use the device in a space application has reduced the climate change impacts of the slot-die coated device. even when gold is used as the top contact.

The majority of LCIA assessments of perovskite have focussed on spin coated lab scale devicesVidal et al. [52], the number of impact categories assessed varies although GWP is the most common since the aim of the solar cell devices is to reduce CO_2 emissions. To compare this work to Vidal's review GWP impact was calculated with 100 % active area and efficiencies as per Table 4. The results for the lab scale device of 2428 g/W_p are at the high end of the literature results as would be expected, the pilot scale device with a gold contact is among the lower end at 583 g/W_p. The pilot scale device with the carbon top contact is only 20 g/W_p, this is lower than in any of the 28 studies reviewed by Vidal which were predominantly spin coated. Since Vidal's review Okoroafor 2022 published a study of inkjet printed perovskite demonstrating the benefits of a small amount of wastage compared to spin coating and using silver as the top contact [40]. Ocoroafor's devices had a GWP of 7.54 g / m^2, this compares with the 3.00 g/m^2 in this study, the increase due to the higher impacts of silver compared with carbon and the energy impacts of the evaporated electron transport layer, C60 in contrast to the spray coated SnO_2 in our devices.

Fig. 4, Fig. 5 and Fig. 6 show the environmental profiles of 1 m^2 of the PSC module with lab-based and R2R slot-die pilot-based methods respectively. In Fig. 4, the gold contact layer is the largest contributor to all of the 18 impact categories GWP (75 %), FPMF (88 %), FDP (69 %),

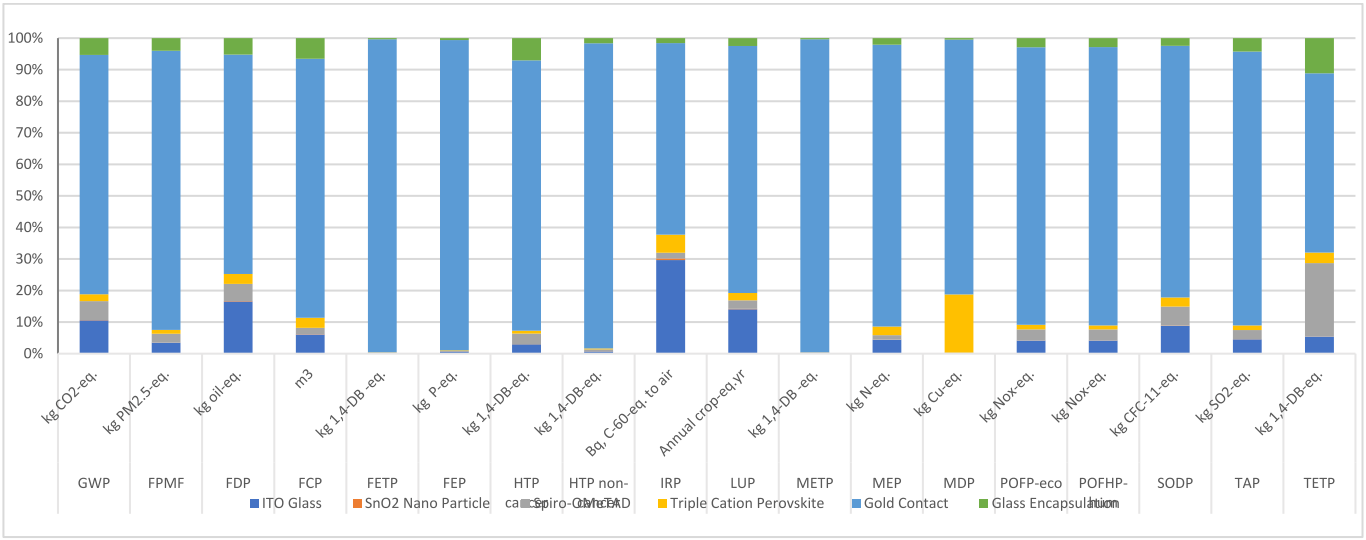

Fig. 4. LCIA of 1 m^2 perovskite solar cell module in the laboratory – comparison impact of each layer.

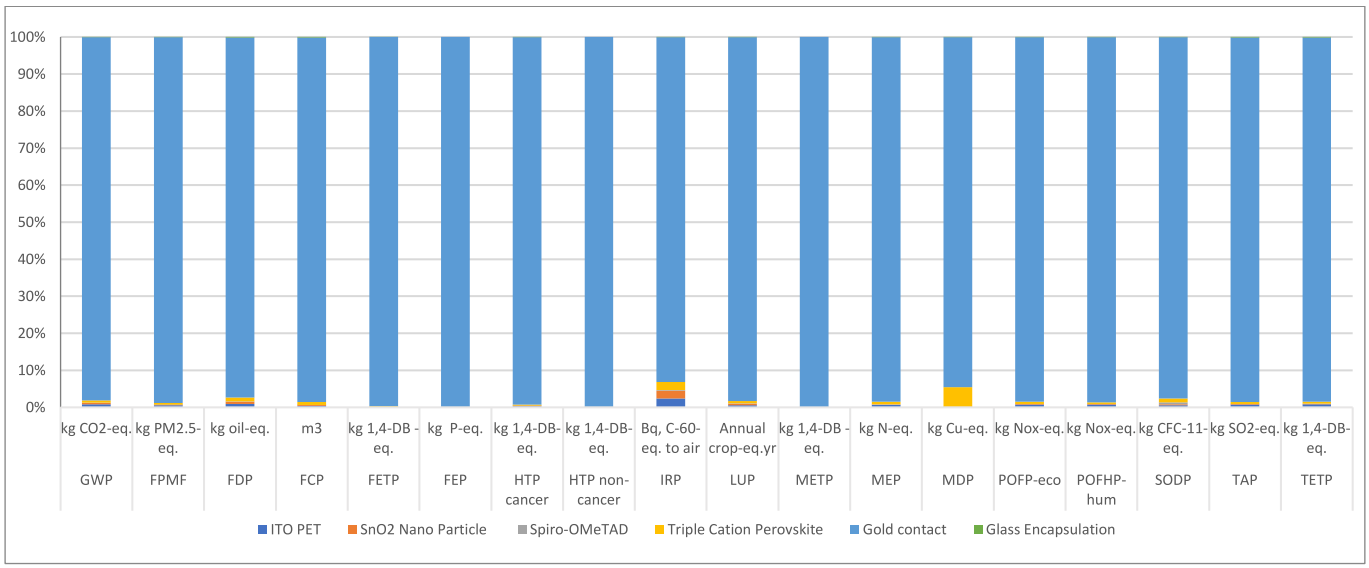

Fig. 5. LCIA of 1 m^2 perovskite solar cell module in the R2R slot-die pilot scale with gold electron – comparison impact of each layer.

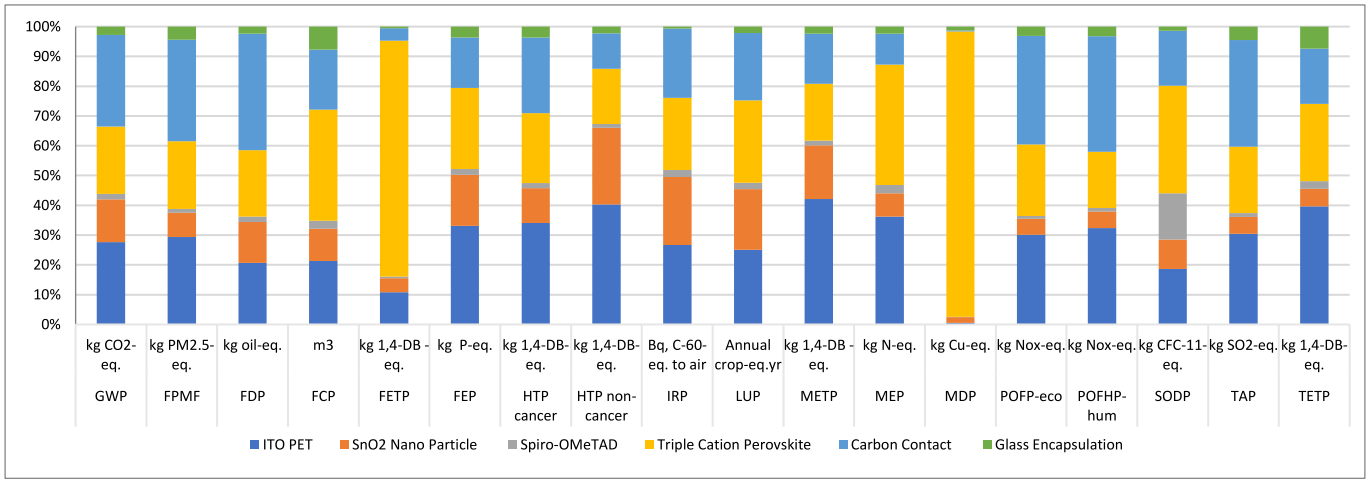

Fig. 6. LCIA of 1 m^2 perovskite solar cell module in the R2R slot-die industry scale with carbon electron – comparison impact of each layer.

FCP (82 %), FETP (99 %), FEP (98 %), HTP cancer (85 %), HTP non-cancer (97 %), IRP (61 %), LUP (78 %), METP (99 %), MEP (8 %), MDP (81 %), POFP-eco (88 %) POFP-hum (88 %), SODP(79 %), TAP (87 %), and TETP (56 %). The reason is due to the high impact of gold [21] and low material efficiency of gold evaporation in the lab-based device which is not recycled.

Fig. 5 demonstrates that when a gold contact electrode is required for performance reasons then the contact layer completely dominates the environmental impact of the module production. To produce 1 kg Au, the GWP is calculated to be around 18000 kg CO2-eq due to the high energy consumption in the mining and comminution stage, and additional process needed [13,39]. The gold causes 95 % of all assessed impacts, which is lower than that in the lab module. This is because the slot-die manufacturing process reduces, wasted materials to less than 1 % and the gold waste is generated during evaporation. The benefit of replacing the gold electrode with a mixed graphite/carbon black electrode is reducing all the assessed impacts which are less than 1 % of these from the lab module (Fig. 4) and 5 % of these from the R2R slot-die with gold contact electrode (Fig. 5). The ITO + PET layer is the largest contributor to 6 of 18 impact categories, FEP (33 %), HTP cancer (34 %), HTP non-cancer (40 %), IRP (26 %), METP (42 %), TETP (39 %). The carbon contact layer is the most significant to impact categories: GWP (31 %), FPMF (34 %), FDP (39 %), POFP-eco (36 %), POFP-hum (39 %), and TAP (35 %), Triple cation perovskite contributes the largest to the impacts of FCP (33 %), FETP (79 %), LUP (27 %), MEP (40 %), MDP (9 %) and SODP (36 %). There is a relatively slight difference among the 6 layers' contribution, especially among the ITO + PET, carbon contact layer, and triple cation perovskite layer. For example the largest contributor of GWP is the carbon contact layer (31 %), followed by ITO + PET (28 %), and the perovskite layer (23 %).

Fig. 6. LCIA of 1 m^2 perovskite solar cell module in the R2R slot-die pilot scale with carbon electron – comparison impact of each layer.

With the only difference between the two R2R slot-die fabrication methods being the utilisation of gold rather than carbon it is shown that gold has a huge environmental impact on device production and research efforts should be focussed on reducing the impacts of this layer by either reducing the amount of gold needed or finding a replacement material for the top contact. Alternative metal contacts such as silver are unsuitable due to a reaction between the silver and the halide ions in the perovskite layer [49]. Carbon contacts avoid this reaction and PCEs of over 20 % have been reported demonstrating the potential for the high efficiencies needed for space applications [59].

4.2. Key contributions to selected impact categories

As described in section 3.1, the potential environmental impacts of the PSC module produced by R2R slot-die are lower than those fabricated by spin coating in the lab thanks to both material use efficiency and alternative materials.

In this section, the breakdown of the major contributors to selected impacts is revealed. The R2R slot-die fabrication technique is chosen due to its higher material use efficiency and lower cost compared with the spin coater from the laboratory. The investigated processes include material acquisition, transportation, and energy consumption during manufacture. Electricity consumption impact is taken from the electricity mix from UK electric grid in 2022. In this analysis, the material used for PSC module production is assumed supplied and produced in China. The transportation includes international sea transportation and lorry transportation within the UK. The data for transportation is from Ecoinvent 3.8. The individual process contribution to impacts of GWP, HTP, MDP, and TETP from R2R slot-die PSC module with a carbon electrode is presented in Fig. 7. Processes or materials with less than 1 % impact are not shown.

4.2.1. Global warming potential

For the slot-die coated device with a carbon top contact electricity consumption by Coatema Smartcoater is the dominate contributor accounting for 53 % of total GWP impact (Fig. 7). The second largest contributor to GWP is logistics which includes both the international ship transportation and lorry transportation. The UK's net-zero strategy has a clear roadmap for electricity carbon intensity to reduce by more than 78 % by 2035[14]. Whilst heavy goods transport has a less transparent strategy UK has a legally binding target of net zero by 2050 and therefore it is anticipated that GWP from both electricity and logistics will reduce significantly in the next decade. The total GWP impact from material acquisition accounts for 29 %, with the solvent 2-Methylanisole being the largest contributor, however as discussed, the overall GWP impact is small compared with other technologies.

4.2.2. Human toxicity potential

Human toxicity potential includes both cancer effects and non-cancer effects. Material acquisition contributes 71 % of total HTP (Fig. 7). Electricity consumption contributes 22 % of the HTP impact, which decreased significantly compared to GWP impact. Within materials, tin oxide (SnO_2) (19.9 %) is the largest contributor followed by ITO (17.3 %) and PET(16.4 %). SnO_2 is the transport conductor layer material. It is noteworthy that HTP impact from lead iodide (PbI) accounts for only 3 % of total HTP despite the concerns around lead in perovskite solar cells [29]. This is in alignment with other LCA studies which note that the lead impacts are minimal due to the small quantity present, however, the soluble nature of the lead could lead to leaching [11,44]. Therefore it is important for both human health and the lifetime of the device that it is encapsulated in such a way that the lead remains intact and is then recycled at the end of life [12].

4.2.3. Metal depletion potential

The impact of MDP of the R2R slot-die carbon electrode PSC module is 0.6 kg Cu-eq /FU dominated by caesium iodide (Fig. 7). This is not because the impact is particularly high but because all the other components are so low, in comparison the lab device had an MDP of 57.3 kg Cu-eq /FU, due to using gold instead of carbon and the poor materials efficiency. When gold is used in the roll-toll slot-die PSC module device rather than carbon electrode MDP increases to 11.6 kg Cu-eq /FU which is dominated by gold use with the caesium iodide only accounting for 4 % of MDP in this scenario.

4.2.4. Terrestrial ecotoxicity potential

Terrestrial ecotoxicology potential is the impact category on how environmental pollutants affect land-dependent organisms and their environment. Material use is also the largest contributor to the TETP impact, which accounts for 73 % of total TETP (Fig. 7). The substrate and TCO layer consisting of ITO and PET contributes 32 % with the next largest impact being the 2-methylanisole (12 %) which is noted as a 'green solvent' since its lower toxicity compared with more commonly used solvent such as chlorobenzene and DMF. The low toxicity of 2-methylanisole means that it can be safe to use during fabrication from a human health perspective. However, to avoid pollution of the land it would be advised to utilise extraction and solvent recovery, this would also enable reuse of the solvent which could balance some of the solvent recovery costs.

4.3. Economic results

The cost of PSC modules fabrication includes material cost including logistic cost, electricity cost, and machine cost.

The economic impacts of the material, electricity usage and depreciation cost of equipment are considered in Fig. 8. Factory overheads and labour cost are out of scope of this work. Mirroring the environmental results, the R2R slot die fabrication in pilot scale method is significantly lower cost than screen coating in the lab scale. To fabricate 1 m^2 PSC module using R2R slot-die with carbon electrode, R2R slot-die with the gold electrode, and spin coating with gold electrode, the cost is 101 €, 206 €, and 13,881 € respectively. The material cost accounts for

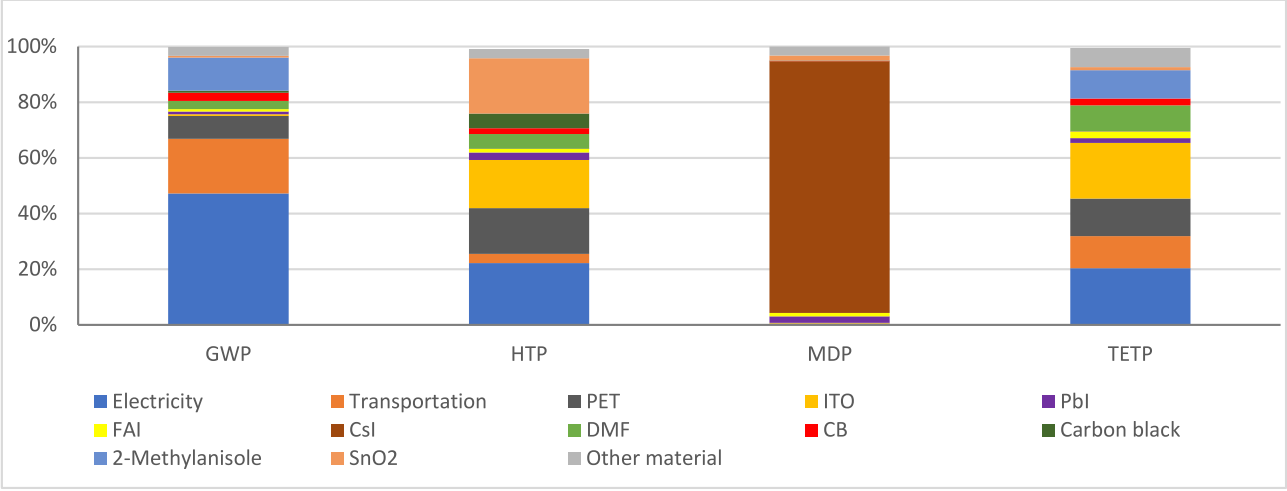

Fig. 7. Percentage breakdown of key contributors to the impacts of roll-to roll slot-die PSC module.

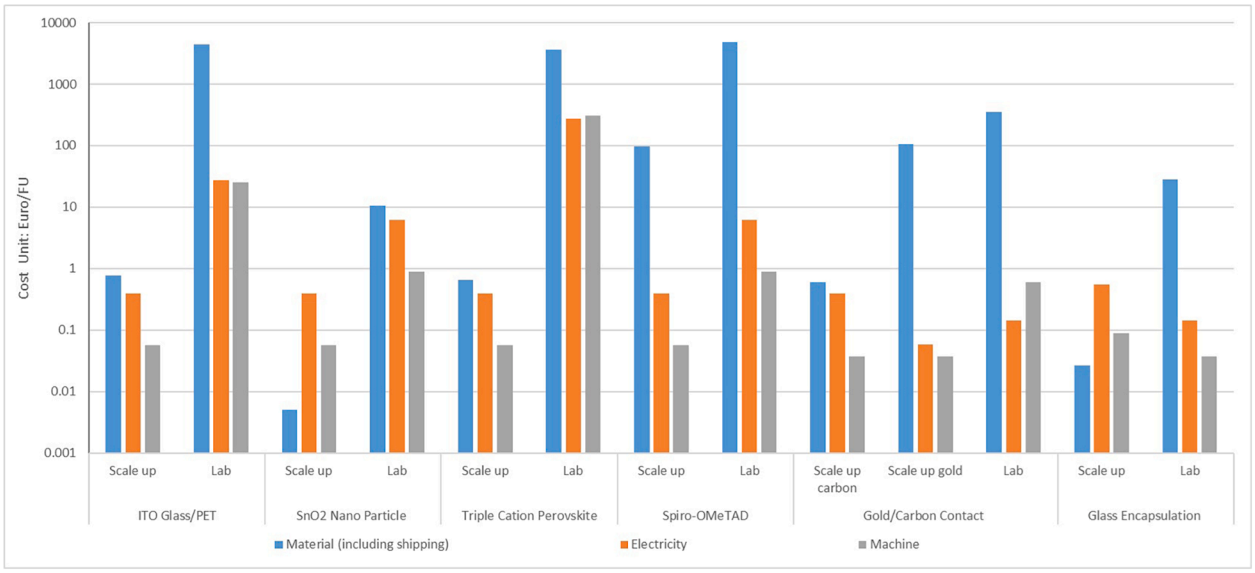

Fig. 8. Costs of material, electricity, and equipment for manufacture 1 m^2 PSC module in R2R slot-die (scale up) and spin coating (lab).

more than 99 % of the total cost of producing PSC module in the R2R slot-die technique (both carbon and gold electrodes), and 95 % of the spin coating technic. The dominating costs of material are the substrate as identified in previous studies [10,41], spiro-OMeTAD as hole transport material, and the gold top contact. At present spiro–OMeTAD is only manufactured for use in academic studies for PSCs. If there is a commercial outlet for it in the future, it is possible that the cost can be reduced. The ITO + PET substrate is also a very high-cost item. For this reason, the sensitivity analysis investigates the impact of changing both the substate and HTL in section 4.

There are some limitations to the analysis of the slot-die coating pilot process which will increase the impacts; firstly non-conformance, whilst materials wastage was considered non-conformance was not included, it is not usual to include this in academic studies but is a requirement when meeting the low carbon module standard as per the Green Electronics Council standard[23]. Secondly, the energy impacts of running the factory were not considered, based on the efficient running of a clean room electricity usage for the room is approximately 3000 kWh per m^2 of the factory per annum [57]. Thirdly the framing of the module is not taken into account. For aerospace applications, this will be part of the structure and therefore framing is not applicable but it should be considered if comparing these results with terrestrial PV standards.

5. Sensitivity analysis

In this section we investigate the impact of the use of alternative materials both for transparent conduction oxides (TCO) and the substrate, the hole transport material as detailed in Table 5.

Table 5
Inventory substrate and TCO materials unit: 1 $m^{2.}$

Glass + TCO	Material	Amount (g)
Soda lime glass + ITO	Soda lime glass	2,769.5
	ITO	0.7
Willow glass + ITO	Willow glass	276.9
	ITO	0.7
PET + ITO	PET	172.5
	ITO	0.7
Willow glass AZO	Willow glass	276.9
	AZO	2.3

5.1. Alternative transparent substrate material

We have shown the potential to replace the gold with a carbon top contact which reduces the environmental impacts by 2 orders of magnitude. In the carbon electrode PSC module, the transparent conductive oxide substrate layer (e.g. PET + ITO) shows the highest impacts in most impact categories. In the gold electrode PSC module, the transparent conductive oxide substrate layer (e.g. PET + ITO/glass + ITO) shows the highest impacts after gold contract layer. Within the perovskite PV community by far, the most commonly employed TCO are patterned ITO and fluorine tin oxide (FTO) coated glass [24,54]. However ITO has high impact of human toxicity potential and indium is a critical raw material, one alternative to replace ITO is aluminium-doped zinc oxide (AZO) [19,33]. The stability is currently one of the challenges for PSC on AZO substrates but the investigation as well as the understanding of the degradation mechanisms remain incomplete [30].

Flexible 'willow' glass supplied by Corning[15], with a thickness is 100 μm has been investigated to replace soda lime glass or PET in space applications[26]. The alternative materials for both transparent conductive layers are presented in Table 5.

Four environmental impacts (GWP, HTP, MDP, and TETP) are chosen to compare ITO + glass with the alternative materials (Fig. 9). In all 4 impact categories, PET, as substrate has the lowest impact followed by willow glass, soda lime glass has the highest impact due to its greater thickness than the willow glass. Examining the TCO layer individually AZO reduces, GWP by 70 %, HTP by 97 %, MDP by 93 %, and TETP by 92 % compared with ITO. However, ITO + PET has a lower GWP and MDP than the alternative composite substrates, because of the lower impacts of PET production.

5.2. Alternative hole transport material

The cost of Spiro-OMeTAD is one of the key barriers for the low-cost future perovskite solar cell production. The current Spiro-OMeTAD has significant cost associated with its complex synthesis and purification. Limited market demand for Spiro-OMeTAD is also a barrier to potential cost reduction in the foreseen future.

While the cost of future production is applicable for all aerospace applications, for space applications in particular, the high-temperature range found in a Low Earth Orbit (LEO) has an adverse effect on the stability and performance of PSCs utilizing the HTL[26]. Therefore, an alternative HTL material should be considered that reduces the cost of

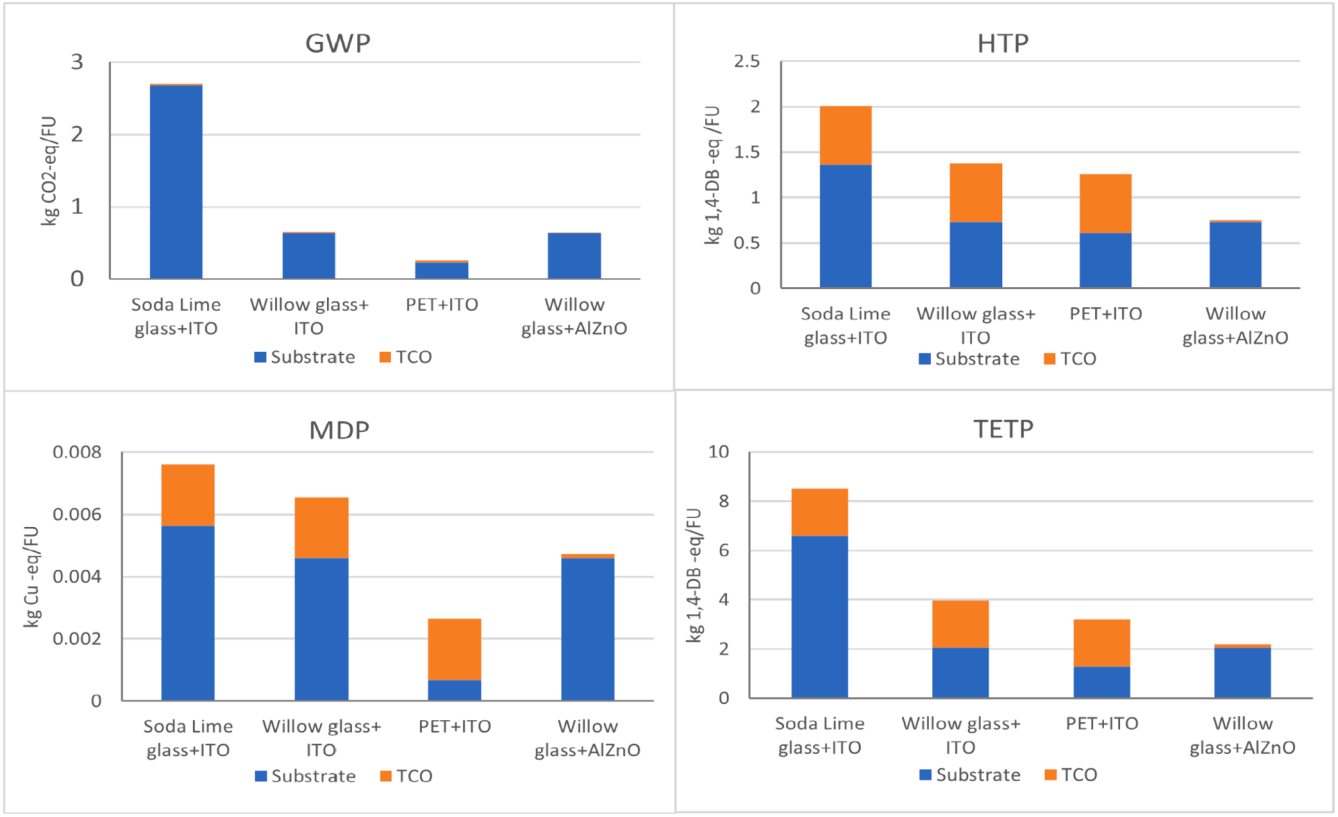

Fig. 9. Comparison of the potential environmental impacts of different substrate and TCO materials of PSC module functional unit: 1 m^2.

fabrication, thus allowing low-cost future production, but that also improves upon the stability of the PSCs with limited sacrifice of PCE.

Here, three common HTL alternatives to Spiro-OMeTAD solution are considered from a cost and environmental viewpoint; POLY(3-HEXYLTHIOPHENE-2,5-DIYL) (P3HT) [55], Poly[bis(4-phenyl)(2,4,6-trimethylphenyl)amine (PTAA) [53]and Copper(I) thiocyanate (CuSCN) [2], which have demonstrated high-efficiency performances of 20.5 % for Spiro-OMeTAD, 17.6 % for P3HT, 22.1 % PTAA and 20.2 % CuSCN). The amount and cost of materials for HTLs are presented in Table 6. It shows dramatic differences among the cost of material options for HTLs. The cost of PTAA is 12,427.1 €/m^2, which is the highest HTL, followed by Spiro-OMeTAD of 96.9 €/m^2. P3HT is the cheapest HTL option among the studied materials. Currently, no industry suppliers for Spiro-OMeTAD, FK209, and 4-*tert*-butylpiridine are found. The only suppliers available for these three chemicals can only offer a small amount for academic/research use.

Interpretation: * is the cost of a small order for academic purposes in the laboratory, no large-scale industry supplier is found.

P3HT has the lowest impacts among all 4 studied HTLs despite the use of chlorobenzene as a solvent. GWP from P3HT is 33 times smaller than it from Spiro OMeTAD, 28 times smaller than it from PTAA, and 24 times smaller than it from CuSCN, however similar performance has not yet been demonstrated [55]. CuSCN has dramatically increased in impacts of HTP, TETP and MDP compared with the other three options.

Regarding applications and stability under aerospace conditions, P3HT has been shown to be thermally stable up to 85 °C [26]and electron/proton radiation stable [36]. However, this stability does come at a cost of efficiency as the PCE of P3HT, which is not yet > 20 %. CuSCN-based PSCs exhibit superior thermal stability compared to spiro-OMeTAD devices, with a small decrease in performance at 85 °C for > 1000 hrs. In preliminary work, CuSCN has also been found to be proton radiation stable at 150 keV. A drawback with CuSCN is the ion migration from the HTL into the electrode and perovskite, degrading performance. There are solutions, such as reduced graphene oxide (r-GO) and aluminium interlayers [2], however, these increase the complexity of moving from the lab into future larger production. Finally, PTAA has been shown to be more thermally stable than Spiro-OMeTAD [43]. its radiation is stable under 20 MeV proton bombardment [32] and is used in perovskite-perovskite tandem cells [7]. The only drawback with PTAA is the current price cost per gram. While this could be reduced if the industry moved towards this HTL, it currently restricts the use of PTAA in larger devices and modules.

Considering economies of scale were out of scope of this work, the niche market of the aerospace industry (Reese 2018) means that demand is unlikely to reach the 1000 W a year described by Matthews et al 2020

Table 6
Inventory hole transport materials unit: 1 m^2.

Hole transport layer	Material	Amount (g)	Cost (€)
Spiro-OMeTAD			**96.9**
	Spiro-OMeTAD	0.05	16.1*
	Chlorobenzene	0.6	2.2E-3
	4-*tert*-Butylpyridin	0.02	0.06
	LI-TFSI	5.6E-3	6.5E-5
	Acetonitrile	0.01	2.2E-5
	FK209	1.8	80.4*
	Acetonitrile	0.1	1.3E-06
CuSCN			**0.3**
	Copper (I) Thiocyanate	56.0	0.3
	Diethyl Sulfide	1.6	0.07
PTAA			**12,427.1**
	PTAA	4.8	12384*
	LiTFSi	12	0.1
	Toluene	1.6	0.03
	Acetonitrile	0.006	8.3E-8
	4-*tert*-butylpiridine	12.0	43.0*
P3HT			**0.1**
	P3HT	16.0	0.09
	Chlorobenzene	1.6	0.006

[35]or even the 100 MW per annum plant described by Culik 2022 Čulík et al. [16], Čulík et al. [17]. Future work will consider a full cost model at a factory size of 1 MW per annum, for aerospace application which can command a higher price than modules for terrestrial power generation. Multicriteria decision analysis can be performed to evaluate the overall sustainability of the alternative PSC module for HAP applications.

6. Conclusion

The goal of this study is to assess the potential environmental impact of the PSC module for HAP application. Two fabrication approaches are compared from spin coating in the lab to R2R slot-die pilot-scale manufacturing based on life cycle assessment and cost methodology. The results of this study indicate that gold electrode is the key barrier to scaling up production of PSC module both from an environmental and economic perspective. The assessed impacts can be reduced by over 90 % by replacing the gold electrode with a carbon electrode. These impacts also have significant reduction by employing R2R slot-die deposition, as it has significantly less waste material during fabrication than the spin coating deposition in the lab.

Analysis of the current UK electricity supply, electricity consumption is the largest contributor to GWP and HTP of PSC module fabrication. Tin oxide, ITO, and PET are the largest material contributing to HTP despite concerns about using lead in the PSC community. CsI from triple cation perovskite dominates the impact of MDP in PSC modules with carbon electrode but it shows a low contribution to other impacts. Besides environmental impacts from material use, material cost is also the main contributor to PSC module cost especially cost from ITO-PET, and Sprio-OMeTAD hole transport layer. After exploring the potential alternative materials of ITO + PET and Sprio-OMeTAD in the sensitivity analysis, we found that there is no environmental benefit to replacing ITO + PET with the studied alternatives. Further work needs to address the optimised thickness of PET with lower environmental impacts and cost without compromising performance. For the HTLs, PTAA shows higher performance and reduced environmental impacts but with the extremely high cost at the current market compared with Sprio-OMeTAD. P3HT show the lowest both in environmental impact and cost but with poor performance. so further studies of technical and economic analysis of potential HTL materials are needed in the future.

Declaration of Competing Interest

The authors declare that they have no known competing financial interests or personal relationships that could have appeared to influence the work reported in this paper.

Acknowledgements

This research was funded by the Engineering and Physical Sciences Research Council (EPSRC), ATIP EP/T028513/1 and ECR Fellowship NoRESt (grant number EP/S03711X/1), We would like to acknowledge Dr. Sean M. Garner from Corning Research & Development Corporation kindly provided us the flexible glass substrates for this work.

Appendix A. Supplementary data

Supplementary data to this article can be found online at https://doi.org/10.1016/j.solener.2024.112602.

References

[1] J.A. Alberola-Borràs, J.A. Baker, F. De Rossi, R. Vidal, D. Beynon, K.E.A. Hooper, T. M. Watson, I. Mora-Seró, Perovskite Photovoltaic Modules: Life Cycle Assessment of Pre-Industrial Production Process. iScience 9 (2018) 542–551, https://doi.org/10.1016/j.isci.2018.10.020.

[2] N. Arora, M.I. Dar, A. Hinderhofer, N. Pellet, F. Schreiber, S.M. Zakeeruddin, M. Grätzel, Perovskite solar cells with CuSCN hole extraction layers yield stabilized efficiencies greater than 20%, Science (80-.). 358 (2017) 768–771, https://doi.org/10.1126/science.aam5655.

[3] A.Z.U.R. Space, SPACE Solar Cells [WWW Document], accessed 4.13.23, https://www.azurspace.com/index.php/en/products/products-space/space-solar-cells, 2023.

[4] J. Barbé, A. Pockett, V. Stoichkov, D. Hughes, H.K.H. Lee, M. Carnie, T. Watson, W. C. Tsoi, In situ investigation of perovskite solar cells' efficiency and stability in a mimic stratospheric environment for high-altitude pseudo-satellites, Journal of Materials Chemistry C 8 (5) (2020) 1715–1721, https://doi.org/10.1039/c9tc04984c.

[5] J. Barbé, D. Hughes, Z. Wei, A. Pockett, H.K.H. Lee, K.C. Heasman, M.J. Carnie, T. M. Watson, W.C. Tsoi, Radiation hardness of perovskite solar cells based on aluminum-doped zinc oxide electrode under proton irradiation, Sol. RRL 3 (2019) 1–8, https://doi.org/10.1002/solr.201900219.

[6] D. Beynon, E. Parvazian, K. Hooper, J. McGettrick, R. Patidar, T. Dunlop, Z. Wei, P. Davies, R. Garcia-Rodriguez, M. Carnie, M. Davies, T. Watson, All-printed roll-to-roll perovskite photovoltaics enabled by solution-processed carbon electrode, Adv. Mater. 2208561 (2023) 2208561, https://doi.org/10.1002/adma.202208561.

[7] H. Bi, Y. Fujiwara, G. Kapil, D. Tavgeniene, Z. Zhang, L. Wang, C. Ding, S. R. Sahamir, A.K. Baranwal, Y. Sanehira, K. Takeshi, G. Shi, T. Bessho, H. Segawa, S. Grigalevicius, Q. Shen, S. Hayase, Perovskite solar cells consisting of PTAA modified with monomolecular layer and application to all-perovskite tandem solar cells with efficiency over 25%, Adv. Funct. Mater. (2023) https://doi.org/10.1002/adfm.202300089.

[8] D. Burkitt, R. Patidar, P. Greenwood, K. Hooper, J. McGettrick, S. Dimitrov, M. Colombo, V. Stoichkov, D. Richards, D. Beynon, M. Davies, T. Watson, Roll-to-roll slot-die coated P-I-N perovskite solar cells using acetonitrile based single step perovskite solvent system, Sustain. Energy Fuels 4 (2020) 3340–3351, https://doi.org/10.1039/d0se00460j.

[9] D. Burkitt, J. Searle, T. Watson, Perovskite solar cells in N-I-P structure with four slot-die-coated layers, R. Soc. Open Sci. 5 (2018), https://doi.org/10.1098/rsos.172158.

[10] M. Cai, Y. Wu, H. Chen, X. Yang, Y. Qiang, L. Han, Cost-Performance analysis of perovskite solar modules, Adv. Sci. (2016), https://doi.org/10.1002/advs.201600269.

[11] I. Celik, Z. Song, A.J. Cimaroli, Y. Yan, M.J. Heben, D. Apul, Life Cycle Assessment (LCA) of perovskite PV cells projected from lab to fab, Sol. Energy Mater. Sol. Cells 156 (2016) 157–169, https://doi.org/10.1016/j.solmat.2016.04.037.

[12] R.G. Charles, A. Doolin, R. Garcia Rodriguez, K.V. Villalobos, M.L. Davies, Circular Economy for Perovskite Solar Cells – Drivers, Energy Environ. Sci, Progress and Challenges, 2023, 10.1039/D3EE00841J.

[13] W. Chen, Y. Geng, J. Hong, H. Dong, X. Cui, M. Sun, Q. Zhang, Life cycle assessment of gold production in China, Journal of Cleaner Production 179 (2018) 143–150, https://doi.org/10.1016/j.jclepro.2018.01.114.

[14] Climate Change Committee, 2020. The Sixth Carbon Budget: The UK's path to Net Zero. Carbon Budg.

[15] Corning, 2019. Corning Willow Glass- fact sheet.

[16] P. Čulík, K. Brooks, C. Momblona, M. Adams, S. Kinge, F. Maréchal, P.J. Dyson, M. K. Nazeeruddin, Design and cost analysis of 100 MW perovskite solar panel manufacturing process in different locations, ACS Energy Lett. 7 (2022) 3039–3044, https://doi.org/10.1021/acsenergylett.2c01728.

[17] P. Čulík, K. Brooks, C. Momblona, M. Adams, S. Kinge, F. Maréchal, P.J. Dyson, M. K. Nazeeruddin, Design and cost analysis of 100 MW perovskite solar panel manufacturing process in different locations, ACS Energy Letters 3039–3044 (2022), https://doi.org/10.1021/acsenergylett.2c01728.

[18] F. De Rossi, J.A. Baker, D. Beynon, K.E.A. Hooper, S.M.P. Meroni, D. Williams, Z. Wei, A. Yasin, C. Charbonneau, E.H. Jewell, T.M. Watson, All printable perovskite solar modules with 198 cm^2 active area and over 6% efficiency, Adv. Mater. Technol. 3 (2018) 2–6, https://doi.org/10.1002/admt.201800156.

[19] S. Devasia, P.V. Athma, R. Raphael, E.I. Anila, Effect of source-substrate distance on the transparent electrode properties of spray pyrolysed aluminium doped zinc oxide thin films, Mater. Today Proc. 59 (2022) 72–78, https://doi.org/10.1016/j.matpr.2021.10.203.

[20] FRONTEX. 2023. *HAPS Market Report -Research study on High-Altitude Pseudo-Satellites*. https://www.frontex.europa.eu/assets/EUresearchprojects/2023/FX_HAPS_WP1_-_Market_Report_V4.pdf.

[21] J. Gong, S.B. Darling, F. You, Perovskite photovoltaics: Life-cycle assessment of energy and environmental impacts, Energy Environ. Sci. 8 (2015) 1953–1968, https://doi.org/10.1039/c5ee00615e.

[22] G. Grancini, C. Roldán-Carmona, I. Zimmermann, E. Mosconi, X. Lee, D. Martineau, S. Narbey, F. Oswald, F. De Angelis, M. Graetzel, M.K. Nazeeruddin, One-Year stable perovskite solar cells by 2D/3D interface engineering, Nat. Commun. 8 (2017) 15684, https://doi.org/10.1038/ncomms15684.

[23] Green Electronics Council, 2023. Criteria for the Assessment of Ultra-Low Carbon Solar Modules.

[24] P. Holzhey, M. Prettl, S. Collavini, C. Mortan, M. Saliba, Understanding the impact of surface roughness: changing from FTO to ITO to PEN/ITO for flexible perovskite solar cells, Sci. Rep. 13 (2023) 1–6, https://doi.org/10.1038/s41598-023-33147-6.

[25] Horowitz, K.A., Remo, T.W., Smith, B., Ptak, A.J., 2018. A Techno-Economic Analysis and Cost Reduction Roadmap for III-V Solar Cells, National Renewable Energy Laboratory.

[26] D. Hughes, Feasibility of perovskite solar cells for space applications, Swansea Univeristy (2023), https://doi.org/10.23889/SUthesis.63570.

[27] D. Hughes, S.M.P. Meroni, J. Barbé, D. Raptis, H.K.H. Lee, K.C. Heasman, F. Lang, T.M. Watson, W.C. Tsoi, Proton radiation hardness of perovskite solar cells utilizing a mesoporous carbon electrode, Energy Technol. 9 (2021), https://doi.org/10.1002/ente.202100928.
[28] HZB, 2022. World record back at HZB: Tandem solar cell achieves 32.5 percent efficiency [WWW Document]. URL https://www.helmholtz-berlin.de/pubbin/news_seite?nid=24348;sprache=en (accessed 4.2.23).
[29] W. Ke, M.G. Kanatzidis, Prospects for low-toxicity lead-free perovskite solar cells, Nat. Commun. 10 (2019) 1–4, https://doi.org/10.1038/s41467-019-08918-3.
[30] F. Khan, I. Fareed, M. Al-Rasheidi, N. Ahmad, A. Al-Ahmed, Z.M. Ahmed, M. Shariq, H. Zahir, Analysis of performance parameters during degradation of triple-cation-based organic–inorganic hybrid perovskite solar cells, Inorg. Chem. Commun. 135 (2022) 109094, https://doi.org/10.1016/j.inoche.2021.109094.
[31] A. Kojima, K. Teshima, Y. Shirai, T. Miyasaka, Organometal halide perovskites as visible-light sensitizers for photovoltaic cells, J. Am. Chem. Soc. 131 (2009) 6050–6051, https://doi.org/10.1021/ja809598r.
[32] F. Lang, M. Jošt, K. Frohna, E. Köhnen, A. Al-Ashouri, A.R. Bowman, T. Bertram, A. B. Morales-Vilches, D. Koushik, E.M. Tennyson, K. Galkowski, G. Landi, M. Creatore, B. Stannowski, C.A. Kaufmann, J. Bundesmann, J. Rappich, B. Rech, A. Denker, S. Albrecht, H.C. Neitzert, N.H. Nickel, S.D. Stranks, Proton radiation hardness of perovskite tandem photovoltaics, Joule 4 (2020) 1054–1069, https://doi.org/10.1016/j.joule.2020.03.006.
[33] H.K.H. Lee, K. Stewart, D. Hughes, J. Barbé, A. Pockett, R.C. Kilbride, K. C. Heasman, Z. Wei, T.M. Watson, M.J. Carnie, J.S. Kim, W.C. Tsoi, Proton radiation hardness of organic photovoltaics: an in-depth study, Sol. RRL 6 (2022), https://doi.org/10.1002/solr.202101037.
[34] Y. Ma, Q. Zhao, A strategic review on processing routes towards scalable fabrication of perovskite solar cells, J. Energy Chem. 64 (2022) 538–560, https://doi.org/10.1016/j.jechem.2021.05.019.
[35] I. Mathews, S. Sofia, E. Ma, J. Jean, H.S. Laine, S.C. Siah, T. Buonassisi, I.M. Peters, Economically sustainable growth of perovskite photovoltaics manufacturing, Joule 4 (4) (2020) 822–839, https://doi.org/10.1016/j.joule.2020.01.006.
[36] Y. Miyazawa, M. Ikegami, H.W. Chen, T. Ohshima, M. Imaizumi, K. Hirose, T. Miyasaka, Tolerance of perovskite solar cell to high-energy particle irradiations in space, Environment. iScience 2 (2018) 148–155, https://doi.org/10.1016/j.isci.2018.03.020.
[37] Y. Mouhamad, S.M.P. Meroni, F. De Rossi, J. Baker, T.M. Watson, J. Searle, E. H. Jewell, Geometrical optimization for high efficiency carbon perovskite modules, Sol. Energy 187 (2019) 129–136, https://doi.org/10.1016/j.solener.2019.05.047.
[38] NESO. National Energy System Operator. 2023. Annual Report and Accounts 2022/2023. https://www.nationalgrideso.com/document/288951/download.
[39] T. Norgate, N. Haque, Using life cycle assessment to evaluate some environmental impacts of gold production, Journal of Cleaner Production 29–30 (2012) 53–63, https://doi.org/10.1016/j.jclepro.2012.01.042.
[40] T. Okoroafor, A. Maalouf, S. Oez, V. Babu, B. Wilk, S. Resalati, Life cycle assessment of inkjet printed perovskite solar cells, Journal of Cleaner Production 373 (2022), https://doi.org/10.1016/j.jclepro.2022.133665.
[41] D. Pourjafari, S.M.P. Meroni, D.P. Domínguez, R. Escalante, J. Baker, A.S. Monroy, A. Walters, T. Watson, G. Oskam, Strategies towards cost reduction in the manufacture of printable perovskite solar modules, Energies 15 (2022) 1–15, https://doi.org/10.3390/en15020641.
[42] M.O. Reese, S. Glynn, M.D. Kempe, D.L. McGott, M.S. Dabney, T.M. Barnes, S. Booth, D. Feldman, N.M. Haegel, Increasing markets and decreasing package weight for high-specific-power photovoltaics, Nature Energy 3 (11) (2018) 1002–1012, https://doi.org/10.1038/s41560-018-0258-1.
[43] F.M. Rombach, S.A. Haque, T.J. Macdonald, Lessons learned from spiro-OMeTAD and PTAA in perovskite solar cells, Energy Environ. Sci. 14 (2021) 5161–5190, https://doi.org/10.1039/d1ee02095a.
[44] L. Serrano-Lujan, N. Espinosa, T.T. Larsen-Olsen, J. Abad, A. Urbina, F.C. Krebs, Tin- and lead-based perovskite solar cells under scrutiny: An environmental perspective, Adv. Energy Mater. 5 (2015) 1–5, https://doi.org/10.1002/aenm.201501119.
[45] H.J. Snaith, Perovskites: The emergence of a new era for low-cost, high-efficiency solar cells, J. Phys. Chem. Lett. 4 (2013) 3623–3630, https://doi.org/10.1021/jz4020162.
[46] Solar, S., 2023. Stratosolar.com/key-enabling-insights [WWW Document].
[47] Spectrolab, Space Cells & CICs [WWW Document] https://www.spectrolab.com/photovoltaics.html#cells_cics 2023 accessed 4.13.23.
[48] L.J. Sutherland, D. Vak, M. Gao, T.A.N. Peiris, J. Jasieniak, G.P. Simon, H. Weerasinghe, Vacuum-free and solvent-free deposition of electrodes for roll-to-roll fabricated perovskite solar cells, Adv. Energy Mater. 12 (2022) 2202142, https://doi.org/10.1002/AENM.202202142.
[49] S. Svanström, T.J. Jacobsson, G. Boschloo, E.M.J. Johansson, H. Rensmo, U. B. Cappel, Degradation mechanism of silver metal deposited on lead halide perovskites, ACS Appl. Mater. Interfaces 12 (2020) 7212–7221, https://doi.org/10.1021/acsami.9b20315.
[50] R. Swartwout, R. Patidar, E. Belliveau, B. Dou, D. Beynon, P. Greenwood, N. Moody, D. deQuilettes, M. Bawendi, T. Watson, V. Bulovic, Predicting low toxicity and scalable solvent systems for high-speed roll-to-roll perovskite manufacturing, Sol. RRL 6 (2022), https://doi.org/10.1002/solr.202100567.
[51] R. Verduci, V. Romano, G. Brunetti, N. Yaghoobi Nia, A. Di Carlo, G. D'Angelo, C. Ciminelli, Solar energy in space applications: review and technology perspectives, Adv. Energy Mater. 12 (2022), https://doi.org/10.1002/aenm.202200125.
[52] R. Vidal, J.A. Alberola-Borràs, N. Sánchez-Pantoja, I. Mora-Seró, Comparison of perovskite solar cells with other photovoltaics technologies from the point of view of life cycle assessment, in: Advanced Energy and Sustainability Research, Vol. 2, Issue 5, John Wiley and Sons Inc., 2021, https://doi.org/10.1002/aesr.202000088.
[53] Y. Wang, L. Duan, M. Zhang, Z. Hameiri, X. Liu, Y. Bai, X. Hao, PTAA as efficient hole transport materials in perovskite solar cells: a review, Sol. RRL 6 (2022), https://doi.org/10.1002/solr.202200234.
[54] Q. Wei, Z. Yang, D. Yang, W. Zi, X. Ren, Y. Liu, X. Liu, J. Feng, S. (Frank) Liu, The effect of transparent conductive oxide on the performance CH3NH3PbI3 perovskite solar cell without electron/hole selective layers, Sol. Energy 135 (2016) 654–661, https://doi.org/10.1016/j.solener.2016.06.044.
[55] N. Yaghoobi Nia, M. Bonomo, M. Zendehdel, E. Lamanna, M.M.H. Desoky, B. Paci, F. Zurlo, A. Generosi, C. Barolo, G. Viscardi, P. Quagliotto, A. Di Carlo, Impact of P3HT regioregularity and molecular weight on the efficiency and stability of perovskite solar cells, ACS Sustain. Chem. Eng. 9 (2021) 5061–5073, https://doi.org/10.1021/acssuschemeng.0c09015.
[56] J. Yang, Q. Bao, L. Shen, L. Ding, Potential applications for perovskite solar cells in space, Nano Energy 76 (2020) 105019, https://doi.org/10.1016/J.NANOEN.2020.105019.
[57] J. Yin, X. Liu, B. Guan, Z. Ma, T. Zhang, Performance analysis and energy saving potential of air conditioning system in semiconductor cleanrooms, J. Build. Eng. 37 (2021), https://doi.org/10.1016/j.jobe.2021.102158.
[58] J.J. Yoo, G. Seo, M.R. Chua, T.G. Park, Y. Lu, F. Rotermund, Y.K. Kim, C.S. Moon, N.J. Jeon, J.P. Correa-Baena, V. Bulović, S.S. Shin, M.G. Bawendi, J. Seo, Efficient perovskite solar cells via improved carrier management, Nature 590 (2021) 587–593, https://doi.org/10.1038/s41586-021-03285-w.
[59] H. Zhang, Y. Li, S. Tan, Z. Chen, K. Song, S. Huang, J. Shi, Y. Luo, D. Li, Q. Meng, High-efficiency (>20%) planar carbon-based perovskite solar cells through device configuration engineering, J. Colloid Interface Sci. 608 (2022) 3151–3158, https://doi.org/10.1016/j.jcis.2021.11.050.
[60] G. Zhao, J. Baker, Effects on environmental impacts of introducing electric vehicle batteries as storage - A case study of the United Kingdom, Energy Strateg, Rev, 2022, p. 40.